

Nonparametric Estimation of Repeated Densities with Heterogeneous Sample Sizes

Jiaming Qiu¹, Xiongtao Dai¹, and Zhengyuan Zhu¹

¹*Department of Statistics, Iowa State University*

Abstract

We consider the estimation of densities in multiple subpopulations, where the available sample size in each subpopulation greatly varies. For example, in epidemiology, different diseases may share similar pathogenic mechanism but differ in their prevalence. Without specifying a parametric form, our proposed approach pools information from the population and estimate the density in each subpopulation in a data-driven fashion. Low-dimensional approximating density families in the form of exponential families are constructed from the principal modes of variation in the log-densities, within which subpopulation densities are then fitted based on likelihood principles and shrinkage. The approximating families increase in their flexibility as the number of components increases and can approximate arbitrary infinite-dimensional densities with discrete observations, for which we derived convergence results. The proposed methods are shown to be interpretable and efficient in simulation as well as applications to electronic medical record and rainfall data.

1 Introduction

Density estimation is one of the most fundamental tasks in statistics and machine learning. A common problem encountered in sciences is to model the distributions of a variable in multiple subpopulations with similar nature, for example the age distributions of patients with different diseases and the precipitation distributions in different regions. Repeated density functions can be modeled as the realizations of a random density element that is subject to the positivity and unit integral constraints. Moreover, density functions are in practice unobserved and are accessed through discrete samples, rendering additional difficulties for data analysis. The primary objective of this work is to address these difficulties and derive reliable yet flexible density estimates for the subpopulations given discrete observations, by borrowing strength from the population in a fully data-driven manner.

Most of the existing work consider random densities that are *completely* observed or are reconstructed from *densely* observed data points. This type of

density objects was first analyzed by [Kneip and Utikal \(2001\)](#) by directly applying functional principal component analysis (FPCA), a technique that has also been applied to analyze the trend of time-varying densities ([Huynh et al. 2011](#); [Tsay 2016](#); [Chu et al. 2018](#)). Recognizing the density constraints, [Delicado \(2011\)](#) and [Petersen and Müller \(2016\)](#) proposed to analyze densities by utilizing one-to-one transformations to map them into an unconstrained space, where the transformed densities are then represented using FPCA and subsequently back transformed into densities. Distinct geometries are generated on the space of densities by different transformations, such as the log hazard and log quantile density transformation ([Petersen and Müller 2016](#); [Kim et al. 2020](#)), log transformations for analyzing densities as compositional data ([Egozcue et al. 2006](#); [Hron et al. 2016](#)); and the square root transformation composed with Riemannian logarithm map ([Srivastava et al. 2007](#)) generating a Hilbert sphere geometry.

We instead consider fitting *sparsely* observed random densities with as few as a handful realizations available. Subpopulations with small sample sizes arise in a number of situations when the sampling mechanism dictates heterogeneous sample sizes. A first situation is when the availability and cost of observation varies among subpopulations ([Wakefield and Elliott 1999](#)), with some groups easy but the rest hard to reach ([Bonevski et al. 2014](#)). This scenario is illustrated by the Medical Information Mart for Intensive Care (MIMIC) data ([Johnson et al. 2016](#)) in our first data application, where patient records are ample for common diseases such as diabetes and coronary heart disease but scarce for uncommon conditions. A second generating mechanism is that the data collection process in different groups had been established for different duration ([Fithian and Wager 2015](#)), which is illustrated by our second data application considering rainfall recorded by weather stations around the Haihe River basin in northern China that differ in the number of years when data are available.

Literature on sparsely observed random densities are scant; a closely related topic is replicated point processes, of which the intensity functions can be normalized into densities. [Panaretos and Zemel \(2016\)](#) considered time-warping densely sampled Poisson point processes under a transportation geometry. Given sparsely sampled replicated point processes, [Wu et al. \(2013\)](#) proposed to pool information over multiple realizations and directly model the intensity functions using FPCA. [Gervini \(2016\)](#) and [Gervini and Khanal \(2019\)](#) considered semi-parametric models to decompose the intensity and the log-intensity functions, respectively.

Our proposal is a nonparametric approach that directly targets the repeated densities, viewing discrete observations from each subpopulation as i.i.d. realizations. Information is pooled over all subpopulations in a two-step fashion. First, we identify low-dimensional structure to parsimoniously approximate the densities using data from subpopulations amply sampled by applying FPCA to the centralized log-transformed densities that lie in an unconstrained L^2 space. When transformed back to densities, the low-dimensional structure make up an exponential family, where the sufficient statistics are the eigenfunctions of the

transformed densities, and each density element is compactly represented by its natural parameter or, equivalently, moment coordinate (Amari 2016). Second, a new and potentially sparsely observed subpopulation is fitted within the approximating family, obtaining maximum likelihood estimate (MLE), and the coordinate estimate is then shrunk towards the population using distributional information, further enforcing information borrowing. A maximum *a posteriori* (MAP) and a best linear unbiased prediction (BLUP) shrinkage are proposed based on the natural parameter and moment coordinates, respectively.

To supply an example, suppose that random densities are generated from the normal distribution family $\mathcal{P} = \{p_{\mu, \sigma} : \mu \in \mathbb{R}, \sigma > 0\}$ with densities $p_{\mu, \sigma}(x) \propto \exp(x(\mu/\sigma^2) - x^2/(2\sigma^2))$ truncated to $x \in [-1, 1]$. Observe that a random element p taking values in \mathcal{P} satisfies $\log p \subset \text{span}\{1, x, x^2\}$ and thus lies in a low-dimensional space; the low-dimensional structure can be recovered by applying dimension reduction techniques such as FPCA on $\log p$. When inferring the distribution of a subpopulation, information borrowing is performed within the low-dimensional space and is analogous to that for the classical linear mixed effects model. Remarkably, the proposed methods estimate the low-dimensional structure and pool information fully nonparametrically without imposing parametric shape assumptions. A worked simulation example is included in [Subsection 3.3](#).

The proposed methods combine the flexibility from non-parametric density estimate and the statistical efficiency and interpretability offered by finite-dimensional parametric inference and information borrowing. Ultimately, fitting a density with sparse observation follows likelihood principles in an estimated exponential family, so the required amount of observations could be substantially fewer than what would otherwise be required for non-parametric estimates. Moreover, the exponential family approximation has the advantage in the interpretability of the sufficient statistics that come from eigenfunctions as well as fast computation. The approximating family increases in flexibility by increasing its dimensions and will fit to a complex density. Rate of convergence under Kullback–Leibler (KL) divergence for the proposed MLE is established under the asymptotics that the number of training subpopulations, the sample size of each subpopulation, and the sample size of the new subpopulation diverge to infinity. This result holds for general infinite-dimensional random densities under smoothness and boundedness conditions. If the random density actually lies in a finite-dimensional exponential family, then the proposed method converges under KL divergence to the truth with a near-parametric rate.

The proposed models and estimation are introduced in [Section 2](#). Numerical properties of the proposed methods are investigated and compared to alternative parametric and nonparametric density estimates in [Section 3](#) under various simulation scenarios. Data illustrations with age-at-admission of ICU patients and historical rainfall data in the Haihe river basin are included in [Section 4](#). Theoretical results are stated in [Section 5](#), and the detailed proofs and additional discussion are included in the Supplemental Materials.

2 Methods and Models

2.1 Data Setup and Goals

Let $\{X_{ij} : j = 1, \dots, N_i, i = 1, \dots, n\}$ be the observations of a continuous variable subdivided into subpopulations $i = 1, \dots, n$; e.g. the age-at-admission to the Intensive Care Unit (ICU) as described in [Subsection 4.1](#) grouped by primary diagnosis. We observe i.i.d. data X_{i1}, \dots, X_{iN_i} from the i th subpopulation with density p_i , $i = 1, \dots, n$, where the densities lie in family \mathcal{P} of densities supported on a compact interval $\mathcal{T} \subset \mathbb{R}$. Here, p_1, \dots, p_n are independent realizations of a random density p taking values in \mathcal{P} , reflecting the fact that different diseases have different characteristics. To emphasize the grouping structure, we refer to p_i as density of the i th *subpopulation*, while the distribution of the random density p as the *population*.

Our goal is to derive universally applicable low-dimensional structure of \mathcal{P} from subpopulations where ample observations are available, e.g. records for more common conditions, and use the structure to estimate an additional density p_0 in a new subpopulation with a few i.i.d. observations X_{0j} , $j = 1, \dots, N$, e.g. for an uncommon disease, where the number of observations N can potentially be small.

2.2 Proposed Repeated Density Estimation

2.2.1 Constructing Approximating Family

We propose to approximate distribution family \mathcal{P} with low rank exponential families utilizing a functional data analytic approach. We discuss here the scenario where the distribution of random density is given, and in [Subsubsection 2.2.4](#) when the distributions are not directly available.

The collection of densities form an infinite-dimensional constraint manifold instead of a Hilbert space. To borrow from the rich literature studying function data as infinite-dimensional objects in a Hilbert space, we follow a transformation approach ([Petersen and Müller 2016](#)) and analyze the transformed densities as elements of a Hilbert space. Applying the centralized log-transformation ([Hron et al. 2016](#)) $\psi : \mathcal{P} \rightarrow L^2(\mathcal{T})$, a positive density $q \in \mathcal{P}$ is mapped into the L^2 space as

$$(\psi q)(t) = \log q(t) - \frac{1}{|\mathcal{T}|} \int_{\mathcal{T}} \log q(x) dx, \quad t \in \mathcal{T}. \quad (2.1)$$

To simplify notations, we use 1 to denote constant function on \mathcal{T} with value 1 , and $e(t) = 1/\sqrt{|\mathcal{T}|}$, $t \in \mathcal{T}$, so that $\int_{\mathcal{T}} \log q(x) dx / |\mathcal{T}| = |\mathcal{T}|^{-1} \langle 1, \log q \rangle = \langle e, \log q \rangle e$.

To derive low rank approximations to the densities, we apply the Karhunen–Loëve expansion to the transformed trajectories $f = \psi p$ in $L^2(\mathcal{T})$, obtaining,

$$f(t) = (\psi p)(t) = \mu(t) + \sum_{k=1}^{\infty} \eta_k \varphi_k(t), \quad t \in \mathcal{T}, \quad (2.2)$$

where $\mu(t) = Ef(t)$ is the mean function, $\eta_k = \int_{\mathcal{T}}(f(t) - \mu(t))\varphi_k(t)dt$ is the k th component score, and (λ_k, φ_k) is the k th eigenvalue–eigenfunction pair of the covariance function $G(s, t) = \text{cov}(f(s) - \mu(s), f(t) - \mu(t))$ satisfying $\lambda_k \varphi_k(t) = \int_{\mathcal{T}} G(s, t)\varphi_k(s)ds$ on $t \in \mathcal{T}$, for $k = 1, 2, \dots$. The eigenfunctions are orthonormal, and the eigenvalues are non-negative and non-decreasing, satisfying $\lambda_1 \geq \lambda_2 \geq \dots \geq 0$.

Low rank approximating density families to \mathcal{P} are then obtained by the back-transformation ψ^{-1} , which take the form of exponential families. The K -dimensional approximation \mathcal{P}_K to \mathcal{P} is an exponential family, defined for $K = 1, 2, \dots$ as

$$\mathcal{P}_K = \{p_{\theta} : \theta \in \mathbb{R}^K, B_K(\theta) < \infty\}, \quad (2.3)$$

containing densities of the form $p_{\theta}(t) = \exp\left(\mu(t) + \sum_{k=1}^K \theta_k \varphi_k(t) - B_K(\theta)\right)$, $t \in \mathcal{T}$, where $B_K(\theta) = \log\left(\int_{\mathcal{T}} \exp\left(\mu(t) + \sum_{k=1}^K \theta_k \varphi_k(t)\right) dt\right)$ is the normalizing constant. Here \mathcal{P}_K is identifiable as will be shown in [Proposition 5.1](#). The random density p is thus approached with its truncated version

$$p_K(t) \propto \exp(\mu(t) + \sum_{k \leq K} \eta_k \varphi_k(t)), \quad t \in \mathcal{T} \quad (2.4)$$

lying in \mathcal{P}_K .

Model components in (2.3) enjoy interpretation within an exponential family, where θ_k is the natural parameter which compactly describes the density, the eigenfunctions φ_k the sufficient statistic, and mean μ the baseline measure. The exponential families \mathcal{P}_K are easy to communicate for downstream tasks as will be illustrated in [Subsection 4.1](#). Analogous to the case for FPCA, the leading eigenfunctions φ_k , $k = 1, \dots, K$ encodes the principal modes of variation in the log-densities, and the η_k are the scores explaining the most variation. Hence, \mathcal{P}_K provides the most parsimonious K -dimensional description of the random (log-)densities, and performing density estimation within \mathcal{P}_K will effectively borrow typical shapes of the densities displayed in the leading eigenfunctions or sufficient statistic.

2.2.2 Fitting Densities within Approximating Families

Given a small sample X_{0j} , $j = 1, \dots, N$ from a new subpopulation, a best fit for the underlying density p_0 is then obtained within the approximating family \mathcal{P}_K . To assess the goodness of fit, various approaches are available from information theory (e.g. [Amari and Nagaoka 2000](#); [Amari 2016](#)), and we adopt the information loss as quantified by the Kullback–Leibler (KL) divergence, defined for two positive densities q_1 , q_2 on \mathcal{T} as

$$D(q_1 \parallel q_2) = \int_{\mathcal{T}} q_1(t) \log\left(\frac{q_1(t)}{q_2(t)}\right) dt. \quad (2.5)$$

KL divergence $D(q_1 \parallel q_2)$ from q_1 to q_2 quantifies the information loss when one approximates q_1 by q_2 . The best approximating element in \mathcal{P}_K minimizing

the KL divergence from the empirical distribution is the maximum likelihood estimate (MLE), defined by $p_{\hat{\theta}} \in \mathcal{P}_K$, where

$$\dot{\theta} = \arg \max_{\theta: B_K(\theta) < \infty} (\theta^T \bar{\varphi}_0 - B_K(\theta)), \quad (2.6)$$

and $\bar{\varphi}_0 \in \mathbb{R}^K$ is the sufficient statistic constructed from the sample X_{0j} , in which the k th element is $N^{-1} \sum_{j \leq N} \varphi_k(X_{0j})$, $k = 1, \dots, K$.

2.2.3 Incorporating Population-level Information

In addition to the typical shapes of random densities, we borrow information from their distribution in the population to reduce variation when fitting a new density, which has significant effects especially if the available sample size is small.

The distribution of p is captured by those of the component scores η_k , $k = 1, \dots, K$. Incorporating such distributional information into the likelihood function, we propose maximum a posteriori (MAP) estimate $\dot{p}_{\text{MAP}} = p_{\dot{\theta}_{\text{MAP}}} \in \mathcal{P}_K$, where the parameter estimate $\dot{\theta}_{\text{MAP}}$ is defined as

$$\dot{\theta}_{\text{MAP}} = \arg \max_{\theta: B_K(\theta) < \infty} (\theta^T \bar{\varphi}_0 - B_K(\theta) + \log \pi(\theta)), \quad (2.7)$$

and π is the unconditional density of the η_k . Analogous to the PACE procedure (Yao et al. 2005), π is constructed using independent normal marginal distributions with mean $E\eta_k = 0$ and variance $\text{Var } \eta_k = \lambda_k$, $k = 1, \dots, K$. Here $\dot{\theta}_{\text{MAP}}$ is interpreted as a shrinkage of the MLE $\dot{\theta}$ towards the population π .

To accommodate non-normal unconditional distributions for the η_k , we propose a second approach to incorporate the population-level knowledge by working with the moment parameterization. The moment parameter, also referred to as the moment coordinate, for an element p_θ in exponential family \mathcal{P}_K is $\xi = (\xi_1, \dots, \xi_K) \in \mathbb{R}^K$, $\xi_k = \int_{\mathcal{T}} \varphi_k(t) p_\theta(t) dt$. Classical result (see Amari 2016) states that the moment parameter is in one-to-one correspondence with natural parameters, satisfying

$$\xi = \partial_\theta B_K(\theta). \quad (2.8)$$

For brevity, we use $\xi(\cdot) : \theta \mapsto \xi(\theta)$ and $\theta(\cdot) : \xi \mapsto \theta(\xi)$ to denote the one-to-one mappings derived from (2.8).

Motivated by the fact that the MLE of natural parameters is the method of moments estimate under moment parameterization, we consider shrinkage estimate based on the the moment parametrization. Let η_0 be the natural parameters of the truncated random densities $p_{0,K} \in \mathcal{P}_K$ of p_0 according to (2.4) and $\tau_0 = \xi(\eta_0) \in \mathbb{R}^K$ the corresponding moment coordinates. We propose to estimate the moment parameter τ_0 by the best linear unbiased predictor (BLUP) of τ_0 given sample sufficient statistics $\bar{\varphi}_0$, defined as

$$\dot{\xi}_{\text{BLUP}} = \text{BLUP}(\tau_0 | \bar{\varphi}_0) \stackrel{\Delta}{=} \text{cov}(\tau_0, \bar{\varphi}_0) \text{var}(\bar{\varphi}_0)^{-1} (\bar{\varphi}_0 - E\bar{\varphi}_0) + E\tau_0$$

$$= \text{var}(\tau_0) \text{var}(\bar{\varphi}_0)^{-1} (\bar{\varphi}_0 - E\tau_0) + E\tau_0, \quad (2.9)$$

where the last equality is due to $E(\bar{\varphi}_0 \mid \tau_0) = \tau_0$ and double expectation. Note that here the covariance and expectation are computed under the joint distribution of $(\tau_0, \bar{\varphi}_0)$. We thus obtain a plug-in estimate $\hat{\theta}_{\text{BLUP}} = \theta(\hat{\xi}_{\text{BLUP}})$ of the natural parameter.

The MAP (2.7) and BLUP (2.9) estimates not only borrow typical shapes of densities via the sufficient statistics φ analogous to the MLE (2.6), but also take advantages of the distribution of the random density through its component scores. We refer to the information embedded in the component scores of log-densities as population-level information. The MAP (2.7) and BLUP (2.9) are, respectively, shrinkage of the MLE (2.6) estimate towards the means under the natural and the moment coordinates. As will be demonstrated in simulation sections and real data examples later, this extra shrinkage turns out to be precious and will reduce information loss when fitting.

2.2.4 Pre-smoothing and unknown distribution of p

Oftentimes the random densities p_1, \dots, p_n and their distribution are not available, but are accessible only through discrete samples $\{X_{ij} : j = 1, \dots, N_i; i = 1, \dots, n\}$. In this case, we apply a *pre-smoothing* step to construct pilot density estimates for the samples, analogous to the approach taken by [Petersen and Müller \(2016\)](#); [Han et al. \(2020\)](#). While many density estimators can be applied here, including kernel density estimate (KDE) and logspline ([Kooperberg and Stone 1991](#)), for theoretical consideration we adopt the weighted KDE

$$\check{p}_i(t) = \left(\int_{\mathcal{T}} \sum_{j=1}^{N_i} \kappa\left(\frac{x - X_{ij}}{h}\right) w(x, h) dx \right)^{-1} \sum_{j=1}^{N_i} \kappa\left(\frac{t - X_{ij}}{h}\right) w(t, h), \quad t \in \mathcal{T} \quad (2.10)$$

to remove boundary bias, where κ is the kernel function and $w(t, h) = 1 / \int_{(t-b)/h}^{(t-a)/h} \kappa(u) du$ is the weight for $\mathcal{T} = [a, b]$. Pilot density estimator is applied on each sample to obtain pre-smoothed densities $\check{p}_1, \dots, \check{p}_n$.

FPCA is then performed on the transformed densities $\check{f}_i = \psi \check{p}_i$, $i = 1, \dots, n$ to obtain sample mean $\hat{\mu}(t) = n^{-1} \sum_{i=1}^n \check{f}_i(t)$ and sample covariance function $\hat{G}(s, t) = n^{-1} \sum_{i=1}^n (\check{f}_i(s) - \hat{\mu}(s))(\check{f}_i(t) - \hat{\mu}(t))$, the associated eigenvalues $\hat{\lambda}_k$ and eigenfunctions $\hat{\varphi}_k$, and the component scores $\hat{\eta}_i \in \mathbb{R}^K$ in which the k th element is $\hat{\eta}_{ik} = \langle \check{f}_i - \hat{\mu}, \hat{\varphi}_k \rangle$ for $k = 1, \dots, n - 1$. Thus we obtain a sample version of the approximating families $\hat{\mathcal{P}}_K$ defined as

$$\hat{\mathcal{P}}_K = \left\{ \hat{p}_\theta : \theta \in \mathbb{R}^K, \hat{B}_K(\theta) < \infty \right\}, \quad (2.11)$$

in which the elements are densities of the form $\hat{p}_\theta(t) = \exp\left(\hat{\mu}(t) + \sum_{k=1}^K \theta_k \hat{\varphi}_k(t) - \hat{B}_K(\theta)\right)$, $t \in \mathcal{T}$, and $\hat{B}_K(\theta) = \log\left(\int_{\mathcal{T}} \exp\left(\hat{\mu}(t) + \sum_{k \leq K} \theta_k \hat{\varphi}_k(t) dt\right)\right)$ is the normalizing constant. Inference for new samples are conducted based on $\hat{\mathcal{P}}_K$ with sufficient

statistic $\hat{\varphi}_{0,\text{ave}} \in \mathbb{R}^K$, in which the k th element is $N^{-1} \sum_{j=1}^N \hat{\varphi}_k(X_{0j})$; here to avoid double over-scripts we use subscript ‘‘ave’’ to denote the average. The distribution of random densities can be accessed via the empirical distribution of the sample component scores. The proposed estimators are then defined using the estimated quantities; in particular, the MLE and MAP within $\hat{\mathcal{P}}_K$ are, respectively,

$$\hat{\theta}_{\text{MLE}} = \arg \max_{\theta: \hat{B}_K(\theta) < \infty} \left(\theta^T \hat{\varphi}_{0,\text{ave}} - \hat{B}_K(\theta) \right), \quad (2.12)$$

$$\hat{\theta}_{\text{MAP}} = \arg \max_{\theta: \hat{B}_K(\theta) < \infty} \left(\theta^T \hat{\varphi}_{0,\text{ave}} - \hat{B}_K(\theta) + \log \hat{\pi}(\theta) \right), \quad (2.13)$$

in parallel with (2.6) and (2.7), where $\hat{\pi}$ is the product of normal densities with mean 0 and variance $s_{\hat{\eta},k}^2$, the sample variance of $\{\hat{\eta}_{ik}, i = 1, \dots, n\}$ for $k = 1, \dots, K$.

For BLUP, $E\tau_0$ and $\text{var}(\tau_0)$ in (2.9) are estimated by the sample mean $\hat{\tau}_{\text{ave}} = n^{-1} \sum_{i \leq n} \hat{\tau}_i$ and covariance matrix $\Sigma_{\hat{\tau}}$ of moment coordinates $\{\hat{\tau}_i = \xi(\hat{\eta}_i) : i = 1, \dots, n\}$ in $\hat{\mathcal{P}}_K$. Further decompose $\text{var}(\bar{\varphi}_0) = E \text{var}(\bar{\varphi}_0 | \tau_0) + \text{var}(\tau_0)$, and estimate the first term via integration by

$$\Sigma_{\hat{\varphi}_{\text{ave}}} = \frac{1}{nN} \sum_{i=1}^n \int_{\mathcal{T}} (\hat{\varphi}(t) - \hat{\tau}_i) (\hat{\varphi}(t) - \hat{\tau}_i)^T \check{p}_i(t) dt,$$

where $\hat{\varphi} : t \mapsto (\hat{\varphi}_1(t), \dots, \hat{\varphi}_K(t)) \in \mathbb{R}^K$ is the sufficient statistic. In combine, the plug-in BLUP estimate for the moment parameters within $\hat{\mathcal{P}}_K$ is obtained as

$$\hat{\xi}_{\text{BLUP}} = \Sigma_{\hat{\tau}} (\Sigma_{\hat{\varphi}_{\text{ave}}} + \Sigma_{\hat{\tau}})^{-1} (\hat{\varphi}_{0,\text{ave}} - \hat{\tau}_{\text{ave}}) + \hat{\tau}_{\text{ave}}, \quad (2.14)$$

and the associated natural parameter $\hat{\theta}_{\text{BLUP}} = \hat{\theta}(\hat{\xi}_{\text{BLUP}})$ is the solution of $\hat{\xi}_{\text{BLUP}} = \partial_{\theta} \hat{B}_K(\theta)$.

When the random densities p_1, \dots, p_n are observed in their entirety, a scenario considered for the interest of theory and referred to as the subpopulations being *completely observed*, it suffices to skip the pre-smoothing step and proceed with the observed densities. in this case, FPCA is performed with the transformed trajectories $f_i = \psi p_i$, $i = 1, \dots, n$ to obtain sample mean and covariance as $\tilde{\mu}(t) = n^{-1} \sum_{i \leq n} f_i(t)$ and $\tilde{G}(s, t) = n^{-1} \sum_{i \leq n} (f_i(s) - \tilde{\mu}(s))(f_i(t) - \tilde{\mu}(t))$, eigenvalues and eigenfunctions $\tilde{\lambda}_k$ and $\tilde{\varphi}_k$, and sample component scores $\tilde{\eta}_{ik} = \langle f_i - \tilde{\mu}, \tilde{\varphi}_k \rangle$, $k = 1, \dots, n-1$. The approximating families $\tilde{\mathcal{P}}_K$ with completely observed densities are defined as

$$\tilde{\mathcal{P}}_K = \left\{ \tilde{p}_{\theta} : \theta \in \mathbb{R}^K, \tilde{B}_K(\theta) < \infty \right\} \quad (2.15)$$

for $K = 1, 2, \dots$, in which the elements are densities $\tilde{p}_{\theta}(t) = \exp \left(\tilde{\mu}(t) + \sum_{k=1}^K \theta_k \tilde{\varphi}_k(t) - \tilde{B}_K(\theta) \right)$, $t \in \mathcal{T}$, and $\tilde{B}_K(\theta) = \log \int_{\mathcal{T}} \exp \left(\tilde{\mu}(t) + \sum_{k \leq K} \theta_k \tilde{\varphi}_k(t) dt \right)$ is the normalizing

constant. The proposed MLE, MAP and BLUP methods can proceed analogously to that within $\hat{\mathcal{P}}_K$. Tilde overscripts are used to denote estimated quantities with fully observed densities.

We refer to the approximating exponential families constructed from the discrete observations from p_1, \dots, p_n as the *training* step to emphasize that the K -dimensional families $\hat{\mathcal{P}}_K$ are flexibly derived from the data despite themselves being parametric families compactly described by a few natural parameters. The random densities p_1, \dots, p_n are referred to as the training densities associated with the training subpopulations, and the corresponding samples as training samples. For performance assessment, we refer to the process constructing density estimates from new observations within the approximating families as the *fitting* or *testing* step, and correspondingly, define testing subpopulation, density, and sample.

2.2.5 Selecting K

The number of components K controls the flexibility of $\hat{\mathcal{P}}_K$ and the key tuning parameter trading off bias and variance when fitting a density. We propose to select K using a penalized approach by considering the Akaike information criterion (AIC), and set $K = K^*$ which minimizes $\text{AIC}(K) \triangleq 2K - 2 \log \hat{p}_K$, where \hat{p}_K is the density estimates within $\hat{\mathcal{P}}_K$ using either (2.12), (2.13), or (2.14). In practice, we observe that the optimal K^* often increases as the fitting sample size increases. Intuitively, the proposed component selection automatically utilizes a more flexible model given a larger sample size, in which case the additional variance that comes with the flexibility is affordable due to the larger sample.

2.3 Practical Considerations

Since the proposed MLE, MAP, and BLUP estimates are performed within exponential families, the optimization tasks in obtaining (2.12)–(2.14) are essentially convex optimization with discrete samples succinctly summarized using the sufficient statistics, and thus the proposed procedure is computationally efficient. For implementation, we adopted `nloptr`, a R version of NLOpt ([Johnson 2020](#)) for optimization, and `fdapace` ([Carroll et al. 2020](#)) for functional data analysis. An R package will be made available on GitHub.

For pre-smoothing, we considered KDE and logspline in numerical examples. For the bandwidth selection for KDE, with the Gaussian kernel, we first applied the method of [Sheather and Jones \(1991\)](#) to obtain optimal bandwidths h_i^* , $i = 1, \dots, n$ for the training samples, and then utilized the median bandwidth $h^* = \text{median}(h_1^*, \dots, h_n^*)$ to each training sample for more stable estimation. Also, we will discuss shortly after [Proposition 5.3](#), it is believed that over-smoothing in the pre-smoothing step with a larger bandwidth h for KDE may help to improve performance.

3 Simulation Studies

We study the numerical properties for the proposed methods and alternative parametric or non-parametric density estimators under various scenarios. Independent training samples $\{X_{ij} : j = 1, \dots, N_i\}$ were drawn from densities p_i , $i = 1, \dots, n$, respectively, where the p_i are independent copies of a random density p . Independent testing samples $\{X_{lj}^* : j = 1, \dots, N_l^*\}$ were then drawn from additional independent copies p_l^* of p for $l = 1, \dots, n^*$. Typically, training samples were generated with larger sample sizes, e.g. $N_i = 100$; while testing samples were smaller with, e.g., $N_l^* = 20$. The small sample sizes in the testing samples pose a challenge for the density estimators compared. The underlying family \mathcal{P} and the distribution of $p \in \mathcal{P}$ will be specified for each scenario. The experiment under each scenario was repeated 500 times.

The proposed methods (2.12), (2.13), and (2.14) are referred to as FPCA_MLE, FPCA_MAP and FPCA_BLUP. For comparisons, we considered the maximum likelihood estimate within the ground truth family \mathcal{P} as an idealized parametric approach, referred to as MLE; non-parametric methods including KDE (Sheather and Jones 1991) and logspline (Kooperberg and Stone 1991); and a repeated point processes (RPP) approach proposed by Gervini and Khanal (2019). These methods do not require training.

The mean KL divergence for the density estimates was used to assess the over-all estimation performance. For density estimate \hat{p}_l^* for the l th testing sample, information loss was evaluated by KL divergence $D(p_l^* \parallel \hat{p}_l^*)$ following definition in (2.5), and we examined the average

$$\text{MKL} = \frac{1}{n^*} \sum_{l=1}^{n^*} D(p_l^* \parallel \hat{p}_l^*)$$

over n^* testing samples to quantify performance. Smaller MKL indicates better estimation performance.

3.1 Flexible Exponential Families

Samples were generated from the truncated normal and the bimodal distributions, where, for the truncated normal scenario, the samples were generated following $N(\mu, \sigma^2)$ truncated on $[-3, 3]$ with $\mu \sim \text{Unif}(-2, 2)$ and $\sigma \sim \text{Unif}(2, 4)$; while for bimodal scenario, the samples were generated according to density $p(x) \propto \exp((4+\theta)x - (26.5+\theta)x^2 + 47x^3 - 25x^4)$, $x \in [0, 1]$ with $\theta \sim \text{Unif}(0, 10)$. In each Monte Carlo experiment, $n = 50$ training samples of size $N_i = 200$ and $n^* = 100$ testing samples with sizes $N = 10$ or 50 were created.

The mean KL divergence in Figure 3.1 shows that the proposed methods using either KDE as pre-smoother or with the complete training densities observed both produce estimates comparable to MLE without requiring explicit specification of a parametric family. Among all the non-parametric density estimators, the proposed methods are shown to be stable and best-performing, especially when the testing samples are small, in which cases the proposed

methods outperformed MLE by borrowing strength among different samples, whereas MLE does not pool information. In particular, for truncated normal family with $N^* = 10$, on average the information loss of the proposed MAP and BLUP were around 20% less compared to that of MLE within ground truth family, and more than 40% less compared to that of KDE.

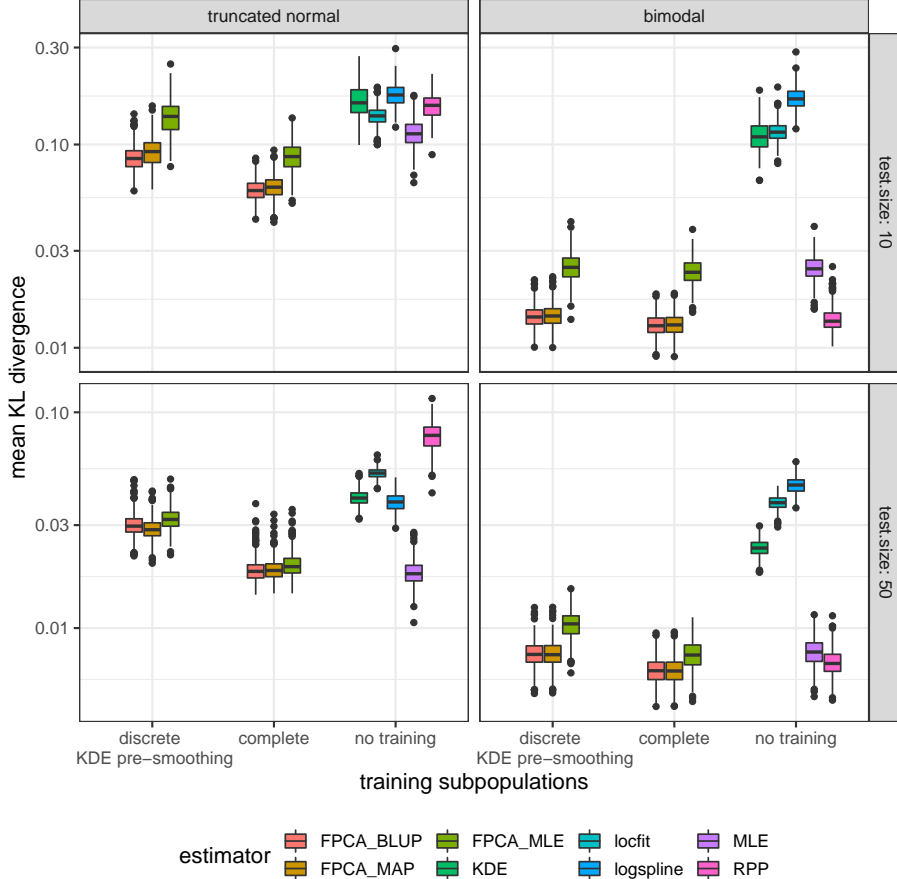


Figure 3.1: Boxplots of mean KL divergence. RPP, repeated point processes approach (Gervini and Khanal 2019); locfit, local polynomial density estimate (Loader 1996); logspline, adaptive logspline (Kooperberg and Stone 1991). Both discrete training samples of sizes $N_i = 200$ with KDE for pre-smoothing and completely observed densities are considered for our proposed approaches, namely FPCA_MLE, FPCA_MAP, and FPCA_BLUP.

3.2 Gaussian Mixture Family

Here we estimate densities for mixture of Gaussian distributions, which forms a multi-modal non-exponential family, so as to further demonstrate the flexibility of the proposed methods and the data-adaptive selection of the number of components used to fit the densities.

The samples were generated following a mixture of three Gaussian distributions with density $p(x) \propto \sum_{l=1}^3 \theta_l \phi((x - \mu_l)/\sigma_l)$ truncated on $x \in [-3, 3]$, where ϕ is the standard normal density, the mixture probabilities $(\theta_1, \theta_2, \theta_3)$ were generated from $\text{Dirichlet}(1/3, 1/3, 1/3)$. For $l = 1, 2, 3$, we generated the mixture mean μ_l from $\text{Unif}(-5, 5)$ and standard deviation σ_l from $\text{Unif}(0.5, 5)$. Here, instead of performing a direct MLE which is known to be unstable for mixture distributions, the expectation–maximization (EM) algorithm in the variant of [Lee and Scott \(2012\)](#) is used as the baseline parametric density estimator.

The left panel of [Figure 3.2](#) compares the relative error of various density estimates to that produced by the EM algorithm. The proposed methods enjoyed the least information loss for all but the largest sample size $N^* = 500$ when EM method became the best. When testing sample size $N^* = 25$, on average, the information loss of proposed MAP and BLUP were 20% less than that of RPP, and they were all at least five times better compared to the EM algorithm. Remarkably, this is achieved by only utilizing the first few components on average, as demonstrated in the right panel of [Figure 3.2](#), which shows that the proposed methods are effective alternatives to the EM algorithm which overcome local maximum issues by performing convex optimization within approximating exponential families. Remarkably, by using the proposed AIC method for component selection, the proposed estimates utilized more components as the size of fitting sample increased, suggesting that the AIC selection adapts to the increased complexity of the underlying family as unveiled by a larger sample. Indeed, the larger the sizes, the more representative the observations from a testing distribution will be for the Gaussian mixture density, which has 8 free parameters in our setup. By using more components, the proposed methods can accommodate the increased complexity shown by the data such as multi-modality, which would otherwise be hidden when fitting with a smaller number of components.

3.3 Random Intercept Family

It is of particular interest to compare the proposed methods with classical parametric approaches when the data are generated according to a random intercept model

$$X_{ij} = A_i + \sigma_e \varepsilon_{ij} \quad (3.1)$$

for stratum $i = 1, \dots, n$ and observation $j = 1, \dots, N_i$ within each stratum, where the A_i follow i.i.d. zero-mean normal distribution with variance σ_a^2 , the ε_{ij} are i.i.d. noise with mean zero and variance one, and σ_a and σ_e are standard deviation parameters regarded as unknown.

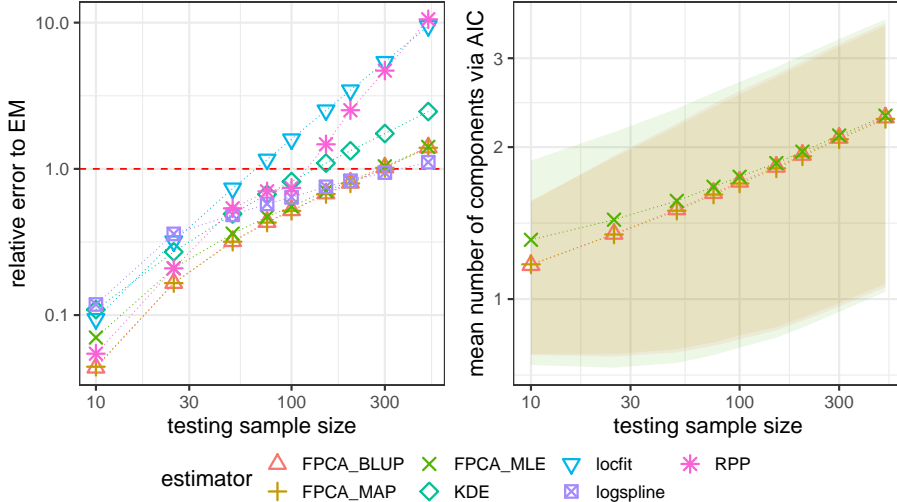


Figure 3.2: The left panel shows the ratio of the average mean KL divergence of compared methods over that of the EM algorithm, where a ratio smaller than 1 indicates better performance than EM. The right panel displays the average number of components K selected by the proposed AIC method, with ribbons indicating one standard deviation around the means. Axes in both panels are drawn in log 10 scale. Size of training samples were 50, and logspline was used as the pre-smoother. RPP, repeated point processes approach (Gervini and Khanal 2019); locfit, local polynomial density estimate (Loader 1996); logspline, adaptive logspline (Kooperberg and Stone 1991); FPCA_MLE, FPCA_MAP, and FPCA_BLUP, the proposed methods in the MLE, MAP, and BLUP variants.

Two cases for the distribution of noise ε_{ij} were considered, a normal distribution and a heavy-tailed t -distribution with 3 degrees of freedom. In each experiment, $n = 100$ training samples were created each with sample size uniformly distributed on the integers between 75 and 100. Next, $n^* = 100$ testing samples each with size ranging from 10 to 20 with equal probability were generated. Standard deviations were set to be $\sigma_a = 1$ and $\sigma_e = 1$. The mean KL divergence were evaluated for the fitted estimates on domain $\mathcal{T} = [-10, 10]$.

We compare against an additional density estimator constructed by the classical linear mixed-effects model approach. Under normality assumption, a parametric density estimator for a new subpopulation given N new observations $\{X_j^* : j = 1, \dots, N\}$ is constructed as the density of $N(\hat{A}, \hat{\sigma}_e^2)$, where $\hat{A} = \bar{X}^*(1 + \hat{\sigma}_e^2 N^{-1} \hat{\sigma}_a^{-2})^{-1}$ is the BLUP for random effect, and $\hat{\sigma}_e$ and $\hat{\sigma}_a$ are residual maximum likelihood estimates obtained from the training samples. This parametric approach is referred to as linear mixed-effects (LME) method in our comparisons.

Results reported in Figure 3.3 shows that KDE performed the worst, the LME method excelled only when the model is correctly specified under normal noises but suffered considerably under t -distributed noises. In contrast, the proposed methods were stable under both setup. In the normal noise case shown in the left panel of Figure 3.3, even the proposed FPCA_MLE performed better than MLE, suggesting the approximating families more closely resemble the underlying truth. Indeed, the underlying density family is one-dimensional, and the proposed FPCA_MLE utilized one component as selected by AIC for more than 80% of the experiments, while the MLE has to estimate two unknown parameters since the variance is unknown. Moreover, as shown in the t noise scenario, the proposed methods outperformed KDE and LME, even if the underlying family is not an exponential family. This shows that the approximation of an arbitrary family through exponential families is fruitful in density estimation.

One shall not be surprised that the LME method outperformed others when the model is well-specified. The strength of LME would be, especially when homoscedasticity would be granted, that the estimates of variance components could pool information from all subpopulations and hence improve performance. In comparison, the MLE method within the ground truth family does not borrow strength across subpopulations. The proposed methods, especially FPCA_MAP and FPCA_BLUP, which utilize population-level knowledge of parameters also outperformed MLE, suggesting that, similar to LME, they successfully pool information from the training samples.

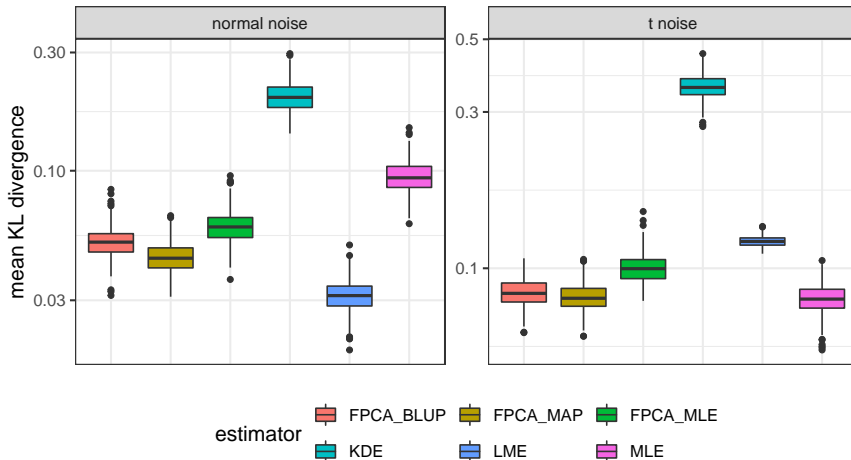


Figure 3.3: Boxplot of Mean KL divergence, one dot for one replication. For FPCA related methods, classic KDE used for pre-smoothing. Normal noise means data generated following model (3.1) and $\varepsilon_{ij} \sim N(0, 1)$, t noise means same model but $\varepsilon_{ij} \sim t_3$.

4 Real Data Applications

4.1 MIMIC Data

In this subsection, we consider the age-at-admission distributions of patients with critical conditions in the Medical Information Mart for Intensive Care (MIMIC) data (Johnson et al. 2016), collected from patients admitted to critical care units at a large hospital in Boston between 2001 and 2012. Ample data points are available to establish a precise non-parametric density estimate for common diseases as shown in the left panels of Figure 4.1, whereas observations for uncommon conditions are scarce and cannot afford flexible non-parametric approaches such as KDE, as displayed in right panels of Figure 4.1. The number of admitted patients with different primary diagnosis are highly heterogeneous in terms of the availability of observations. Estimating the densities in the hard-to-observe subpopulations of patients with uncommon conditions is the emphasis in our analysis.

Gender and diagnosis code (ICD9) combination was used to define the subpopulations, excluding birth-related, unclassified, or unspecified diagnosis. We analyzed a total of 940 subpopulations with more than 5 observations each, among which 75 subpopulations with at least 75 observations were used as the training set and the rest 865 subpopulations as the testing set. For example, as shown in the left panels of Figure 4.1, 109 female patients with juvenile type diabetes with ketoacidosis (DMI ketoacd uncontrold) forms a training sample. The right panels of Figure 4.1 display four testing samples; for example, the last testing sample is formed by 27 male patients with abdominal aortic aneurysm rupture (Rupt abd aortic aneurysm). This is a highly dangerous condition that is actually more prevalent than the available data appears due to low survival — approximately only 25% of patients with a rupture reach hospital alive and survive repair surgery (Aggarwal et al. 2011). We focused on estimating the densities supported in the age range of [14, 85]. The proposed methods utilized KDE as the pre-smoother with the bandwidth set to the median of bandwidths in the training samples selected by the method of Sheather and Jones (1991).

As illustrated in right panels of Figure 4.1, the proposed density estimates produced sensible results given small test samples, which were smoother than the estimates given by KDE and avoided sudden multiple modes. For example, for male aneurysm ruptured patients with only 27 observations (bottom right subpanel of Figure 4.1), KDE under-smoothed severely and produced three suspiciously narrow modes, while all three of our estimates agreed on a single mode. For the male morbid obesity patients, the BLUP and MAP estimates were shrunk towards the population and settled on flatter curves with modes shifted to relative older age compared to MLE.

The modes of variation in the density functions obtained by varying each of the first three natural parameters of \hat{P}_K are shown in the left panels of Figure 4.2. The first three modes of variations correspond to a shift in the age distribution towards the old, the elderly, and the middle age, respectively. This suggests the existence of latent disease characteristics that affect the age profiles

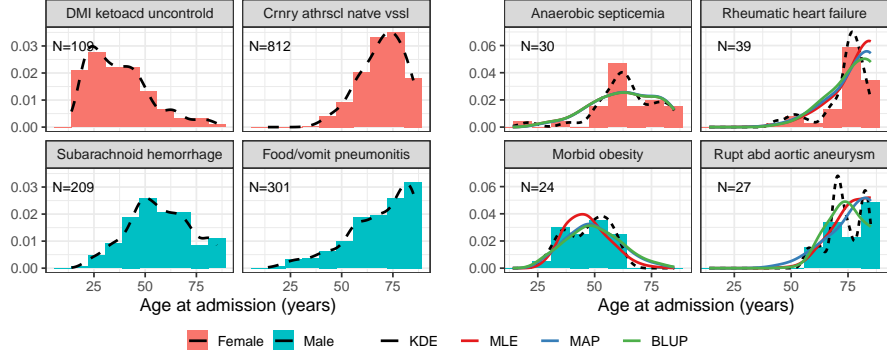


Figure 4.1: Each panel shows the age-at-admission distribution of either male or female patients under a different primary diagnosis, defining a subpopulation. Four training subpopulations with ample observations were shown in the left panels, and four testing subpopulations with scarce observations are shown in the right panels. Along with the KDE, the proposed density estimates MLE, MAP and BLUP are displayed for the testing subpopulations. The sample size is labeled in each panel. KDE, kernel density estimate; MLE, MAP and BLUP, the proposed density estimates.

of different conditions.

The effects of shrinkage in the proposed MAP and BLUP estimators are demonstrated in the right panels of Figure 4.2 for the four rare conditions displayed in the right panels of Figure 4.1. Subpopulations with smaller sample sizes were typically shrunk more towards the population mean using the MAP and BLUP methods that pool population information from the training samples, in which case the estimate differed more notably from the MLE within the approximating family.

To assess the density estimates, we consider cross-entropy which also targets the information loss instead of the KL divergence, since the underlying densities are unknown. Given any density estimator \hat{p} , we approach the cross-entropy $H(p, \hat{p}) \triangleq -E_p \log \hat{p}$, which is the quantity in $D(p \parallel \hat{p})$ that depends on the estimate \hat{p} , by an unbiased leave-one-out estimate

$$H_{\text{LOO}}(p, \hat{p}) \triangleq -\frac{1}{N} \sum_{j \leq N} \log \hat{p}_{-j}(X_j), \quad (4.1)$$

where \hat{p}_{-j} is a density estimate constructed with all but the j th observations. Smaller cross-entropy indicates better estimates. A summary of cross-entropy applied on 844 testing samples using the proposed methods and KDE are reported in Table 1. Occasionally KDE resulted in non-finite cross entropy, leading to a smaller number of samples reported.

Results summarized in Table 1 shows that the proposed methods generated

density estimates that better reflect sample information compared to KDE by having smaller mean and median cross-entropy, and also smaller standard deviations. To quantify the sensitivity w.r.t. the training subpopulations, we partitioned the training samples into 5 folds, held out one fold at a time in the training step, fitted the densities for the testing samples, and reported the range of the five mean cross-entropies for a sensitivity measure. The proposed methods are shown to be insensitive to varying training subpopulations, which suggests that using a subset of the training samples is sufficient for our methods to capture the major structure of the underlying family.

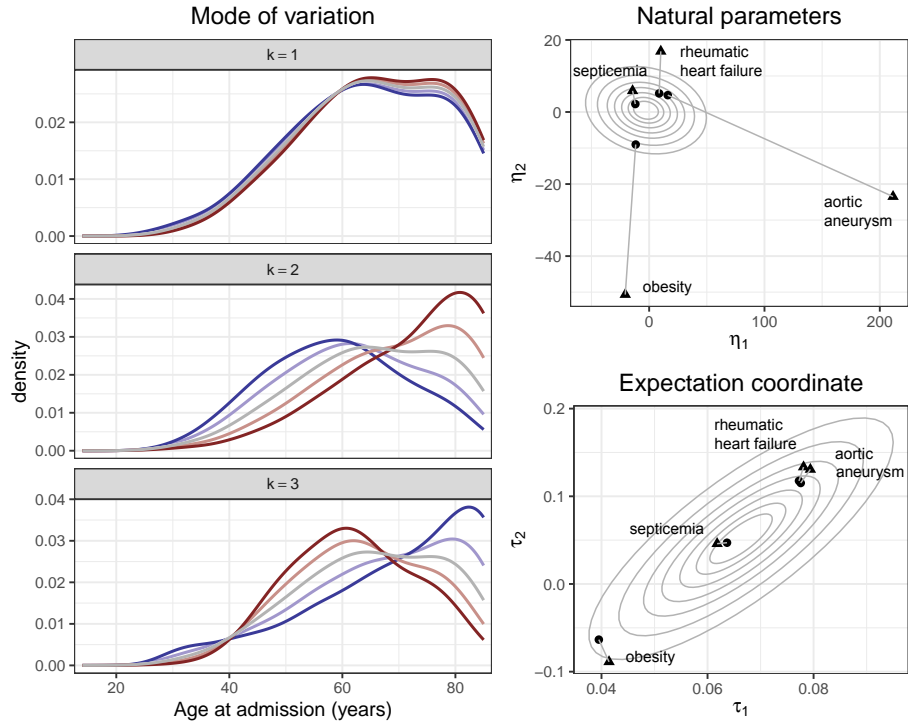


Figure 4.2: Left: mode of variation by varying each of the first three natural parameters of the estimated family $\hat{\mathcal{P}}_K$, blue is lower, red is higher. Right: for the four sparsely observed subpopulations mentioned in the right panels of Figure 4.1, the MLE parameter estimates (triangles) are shrunk in the natural parameter space and the expectation coordinate space w.r.t. the population distribution of training component scores (elliptical contours), producing the corresponding MAP (dots, upper right) and BLUP (dots, lower right) estimates.

Table 1: Cross-entropy (4.1) of different estimators applied on the MIMIC data, stratified by size of testing samples, where the number of testing samples involved is listed as n^* . The sensitivity of proposed methods are the range of the mean cross-entropy across 5 experiments, each holding out one of five folds in the training samples.

size	n^*	estimator	mean	median	sd	sensitivity
(0,10]	423	MLE	4.603	4.268	1.616	0.062
		MAP	4.129	4.072	0.423	0.013
		BLUP	4.111	4.078	0.359	0.039
(10,35]	343	KDE	5.558	4.713	2.418	-
		MLE	4.034	4.027	0.323	0.015
		MAP	3.969	3.978	0.250	0.005
(35,75]	78	BLUP	3.965	3.963	0.241	0.017
		KDE	4.155	4.139	0.371	-
		MLE	3.933	3.991	0.216	0.013
	341	MAP	3.920	3.970	0.209	0.004
		BLUP	3.921	3.967	0.208	0.008
		KDE	3.990	4.021	0.222	-

4.2 Precipitation Return Level Estimation

In this section we analyze the precipitation data in the Haihe region to illustrate the versatility of the proposed methods, which can provide good estimates for both the main body of the density function and tail probability after proper transformation. We demonstrate that our proposed methods can borrow information from stations with longer records to construct approximate distribution families for annual maxima of hourly rainfall, which lead to better estimates of densities and return levels for those stations having shorter records.

Predicting the likelihood of extreme precipitation is of great importance because of the serious damage it can cause to economy and social life. Here we are in particular interested in heavy rainfall during short time period. As China's urbanization process rapidly proceeds, the city drainage systems lag behind and lead to dangerous urban flooding especially when there is extreme precipitation; an example is a record-breaking extreme rainfall happened in Beijing, July 21, 2012 with an hourly rainfall rate exceeding 85 mm (Zhang et al. 2013). The likelihood of extreme precipitation event in a certain region can be quantified using the T -year return level, which is defined as the level expected to be exceeded once in T years. Under stationary and independent assumptions, the T -year return level is the $1 - 1/T$ quantile of the marginal distribution of annual hourly maximum precipitation (see, e.g., Reiss and Thomas 2007). Sample quantile is a straight forward estimate for small T , which is referred to as the empirical return level, but this approach requires more than T data

points available. Otherwise, distribution models are necessary for estimating the return level for longer return periods.

We focus on estimating the 5- to 30-year return levels at various locations in the Haihe River basin, which is a vital region in northern China and include mega-cities such as Beijing and Tianjin. Precipitation data from 232 weather stations around Haihe River basin during 1961 to 2012 is available from the National Meteorological Information Center (NMIC) and China Meteorological Administration (CMA) and are used for this analysis. All the 232 stations investigated have at least 30 years of records.

The heterogeneity in the availability of meteorological records is a common problem especially in the developing world, where weather stations with data can be traced back in time may be limited, making the inference in many regions heavily rely on model assumptions that are vulnerable to misspecification. Moreover, most classical approaches depend on asymptotic results from extreme value theory; for example, the block maxima method with generalized extreme value distribution (GEV) is built upon the limiting distribution of block maxima (Fisher and Tippett 1928; Gnedenko 1943), which may not be a good approximation when the sample size is not very large. Furthermore, generalization of such models to incorporate spatial dependency are typically non-trivial, sophisticated modeling is required to borrow information from nearby stations (see, e.g., [Yin et al. 2018](#)).

Our proposed methods are applied to handle the heterogeneity in record lengths. We obtained approximating families from the longer records in stations established earlier and used these families to fit shorter records from stations established more recently. Furthermore, the population-level information extracted from the longer records will help reduce variance in estimation especially when the data from the fitting station is relatively short.

We targeted the distribution of the annual maximum rainfall per hour, where each station defines subpopulation. For example, Beijing station had 52 years of data available, and the 52 annual maxima are denoted as $\{Y_{1j}, j = 1, \dots, 52\}$. As the distribution of precipitation is heavily right-skewed with heavy right-tail, the pre-smoothing density estimates could be zero within the working domain, creating an issue when we calculate the log-density. To address this issue, we applied log-scaling by first working with densities of log-precipitation $X \stackrel{\Delta}{=} \log Y$, and then applying change of variables to construct approximating families in the original scale of the precipitation. More details of the scaling approach is described in the [Appendix](#).

To compare the performance of the proposed methods with standard approaches, we consider the two performance measures, namely the return levels estimation and the information loss. To imitate the situation of newer weather stations having shorter records, we randomly selected $n = 50$ stations as training sites and used the full records in these stations for training. Another $n^* = 100$ testing sites were randomly selected from the rest of the stations and a random sample of 10 consecutive years was selected from each testing site for fitting. Density estimates and 5- to 30-year return levels were obtained from non-

parametric approaches including our proposed approaches and standard KDE, as well as parametric approaches of maximum likelihood estimates within the family of Gamma and GEV distribution. The performance metric we used to evaluate density estimation was information loss as assessed via cross-entropy (4.1), and that for return level estimates is the relative difference of the estimates and the empirical return levels that are obtained from full records in the testing stations. The entire process was repeated 10 times with the overall average cross-entropies reported in [Table 2](#) and the relative differences of the return levels averaged over the stations displayed in [Figure 4.3](#).

The information loss measures the overall fit, and the proposed methods in the MLE, MAP, and BLUP variants are all significantly better than the KDE and GEV approaches. The estimates using Gamma family of distributions were comparable to our results in terms of information loss but underperformed the MAP and BLUP methods which borrow information from the population. For return level estimation, as shown in [Figure 4.3](#), the proposed MAP and BLUP methods had the least variation compared to MLE, Gamma and GEV methods, where the last three methods do not pool information. For shorter (5- and 10-year) return level, the bias of all methods were comparable, but for longer (20- and 30- year) return level, the bias of our methods were significantly smaller than Gamma and GEV methods. In sum, our proposals had the best performance in estimating the return levels as well. Hence, the proposed methods provide better fits compared to classical approaches in both the bulk and the tail parts of the distributions and lead to better quantification of interesting characteristics of the distribution such as return levels from a few discrete observations.

These numerical results come as a positive surprise, as we only used 10 years of records at the testing sites and yet were able to obtain good estimates for 20- and even 30-years return levels. It appears to be a generally successful approach for the proposed approaches to estimate the tail structure from the data rather than relying on assumptions, and borrow information from the population enforced through parameter shrinkage.

Table 2: Cross-entropy (computed by (4.1)) of different estimators applied on the Haihe rainfall data fitted with decennial records over 10 repeated experiments. MLE, MAP, and BLUP, the proposed methods; KDE, kernel density estimate; Gamma, density fit within a Gamma distribution; GEV, density fit within a GEV family using `fevd` from `extRemes` package ([Gilleland and Katz 2016](#)).

	MLE	MAP	BLUP	KDE	Gamma	GEV
mean	6.366	6.253	6.267	6.934	6.296	6.716
sd	0.046	0.031	0.036	0.118	0.031	0.100

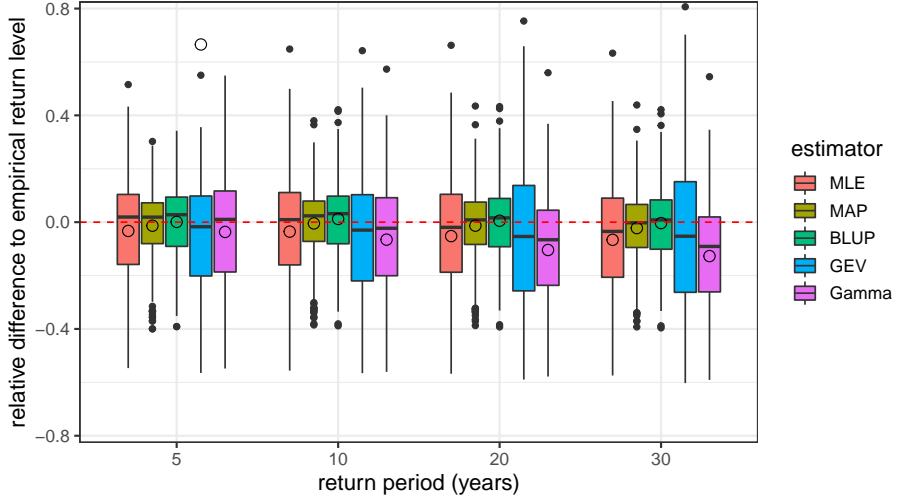


Figure 4.3: Relative differences of estimated return levels using decennial records compared to empirical ones using full records (≥ 30 years) for testing weather stations. Each solid dot represent the average relative difference at a station averaged over Monte Carlo experiments, while each hollow circle represents the mean over all stations. Estimates closer to the red zero-reference line are better. The GEV had some extreme over-estimate outliers pulling its mean errors outside plotting range.

5 Theoretical Results

Here we state the theoretical results for the proposed methods including the identifiability of the approximating families, consistency of MLE within those families, and consistency of the component scores. Proofs and additional discussion are included in the supplementary materials.

Densities in the underlying family are required to be smooth and uniformly bounded away from zero and infinity.

(A1) All densities $q \in \mathcal{P}$ are continuously differentiable. Moreover, there is a constant $M > 1$ such that, for all $q \in \mathcal{P}$, $\|q\|_\infty, \|1/q\|_\infty$ and $\|q'\|_\infty$ are bounded above by M .

5.1 Identifiability

Firstly, we show that the approximating families \mathcal{P}_K , $\tilde{\mathcal{P}}_K$, and $\hat{\mathcal{P}}_K$ as defined in (2.3), (2.15), and (2.11) are identifiable due to the orthogonality of the sufficient statistics. Given any covariance function G supported on $\mathcal{T} \times \mathcal{T}$, we define the associated integral operator $\mathcal{G} : L^2(\mathcal{T}) \rightarrow L^2(\mathcal{T})$ as

$(\mathcal{G}g)(s) = \int_{\mathcal{T}} G(s, t)g(t)dt, s \in \mathcal{T}$, and define its rank to be the dimension of its image $\{\mathcal{G}g : g \in L^2(\mathcal{T})\}$, denoted as $\text{rank } \mathcal{G}$, which may be infinity.

Proposition 5.1. Under [\(A1\)](#), \mathcal{P}_K is identifiable for $K = 1, \dots, \text{rank } \mathcal{G}$ and $\tilde{\mathcal{P}}_K$ is identifiable for $K = 1, \dots, \text{rank } \tilde{\mathcal{G}}$. Moreover, $\hat{\mathcal{P}}_K$ is identifiable for $K = 1, 2, \dots, \text{rank } \hat{\mathcal{G}}$ as long as $\check{p}_1, \dots, \check{p}_n$ are strictly positive on \mathcal{T} .

5.2 Consistency of MLE

The proposed MLE estimates within low-dimensional approximating family $\hat{\mathcal{P}}_K$ are shown to be consistent here. The MLE is computed with an additional i.i.d. sample X_1, \dots, X_N of size N , of which the density p is an independent copy of the random density. The approximating family $\hat{\mathcal{P}}_K$ is obtained from n discretely observed training subpopulations each with $N_i \geq m$ observations. Theoretical results for this scenario that represents most practical computation are presented here, deferring results for MLE obtained within \mathcal{P}_K and $\tilde{\mathcal{P}}_K$ to the Supplementary Materials. For simplicity of notation, we use $\hat{p} = \hat{p}_{N,K} \in \hat{\mathcal{P}}_K$ to denote the MLE density estimate with parameter $\hat{\theta} = \hat{\theta}_{N,K}$ defined in [\(2.12\)](#).

We base our consistency results on the following assumptions imposed on the covariance of the log-transformed random density.

(C1) For process $f = \psi p \in L^2(\mathcal{T})$, the eigenvalues and eigenfunctions of the integral operator \mathcal{G} associated with the covariance function G satisfy, as $J \rightarrow \infty$,

$$\begin{aligned} \left(\sum_{k=1}^J \|\varphi'_k\|_\infty \right) \left(\sum_{k>J} \lambda_k \right) &= O(1), \\ \left(\sum_{k=1}^J \|\varphi'_k\|_\infty \right)^{2/3} \left(\sum_{k>J} \lambda_k \right) &= o(1). \end{aligned}$$

(C2) For all $k = 1, \dots, \text{rank } \mathcal{G}$, the non-zero eigenvalues are distinct and satisfy $\delta_k \stackrel{\Delta}{=} \inf_{l \neq k} |\lambda_k - \lambda_l|/2 > 0$; the estimated eigenfunctions are properly aligned so that $\langle \varphi_k, \check{\varphi}_k \rangle \geq 0$ and $\langle \varphi_k, \hat{\varphi}_k \rangle \geq 0$.

Condition [\(C1\)](#) ensures that the high frequency eigenfunctions are not overly bumpy relative to the amount of information they are carrying as quantified by the eigenvalues, so that the trajectories can be reasonably presented with the first few components. Condition [\(C2\)](#) imposed on the eigenvalues and eigenfunctions is standard for simplifying presentation. We assume $\text{rank } \mathcal{G} = \infty$ in discussion hereafter unless otherwise stated.

5.2.1 Pre-smoothing

Conditions [\(A1\)](#), [\(C1\)](#), and [\(C2\)](#) in combine are sufficient for consistency of MLE within \mathcal{P}_K and $\tilde{\mathcal{P}}_K$ as shown in [Theorem S4.2](#) of supplementary materials.

When discrete training samples and pre-smoothing are involved, the following conditions in parallel to (D1), (D2), and (S1) in Petersen and Müller (2016) are also required. To state the conditions, let $q \in \mathcal{P}$ be a fix density; the conditions here are imposed on family \mathcal{P} but not on the distribution of the random density p . Further, let \check{q} to be the corresponding pre-smoothed density, e.g. according to the weighted KDE defined in (2.10).

(D1) There exists a positive sequence $b_N = o(1)$ as $N \rightarrow \infty$, such that based on an i.i.d. sample of size N from density $q \in \mathcal{P}$, the density estimator \check{q} satisfies $\check{q} \geq 0$, $\int_{\mathcal{T}} \check{q} = 1$ and

$$\sup_{q \in \mathcal{P}} E(\|\check{q} - q\|_2^2) = O(b_N^2).$$

(D2) There exists a positive sequence $a_N = o(1)$ as $N \rightarrow \infty$ and some $R > 0$ such that based on an i.i.d. sample of size N from a population for which the density is $q \in \mathcal{P}$, density estimator \check{q} satisfies $\check{q} \geq 0$, $\int_{\mathcal{T}} \check{q} = 1$ and

$$\sup_{q \in \mathcal{P}} P(\|\check{q} - q\|_{\infty} > Ra_N) \rightarrow 0 \text{ as } N \rightarrow \infty.$$

(S1) Let \check{q} be a density estimator satisfying (D2) and $N_i = N_i(n)$, $i = 1, \dots, n$ be the sample sizes in the training subpopulations. There exists a sequence of lower bounds $m(n) \leq \min_{1 \leq i \leq n} N_i$ such that $m(n) \rightarrow \infty$ as $n \rightarrow \infty$ and

$$n \sup_{q \in \mathcal{P}} P(\|\check{q} - q\|_{\infty} > Ra_m) \rightarrow 0,$$

where \check{q} is obtained with sample size $N(n) \geq m(n)$.

Conditions (D1), (D2), and (S1) basically indicate that the pilot density estimator performs well uniformly provided with sufficiently large samples. Here (D1) is a uniform MISE requirement, (D2) requires the L^{∞} error to be $O_p(a_m)$, and (S1) is a requirement for the rate of sample sizes as the number of samples increases, so that one can derive uniform rates of convergence for the pre-smoothed training densities and log-densities under the L^{∞} norm.

The following proposition generalizes a version from Petersen and Müller (2016) and states that the weighted kernel density estimate (KDE) in (2.10) fulfills all the conditions required for the pre-smoother given proper bandwidths and that a kernel assumption (K1) holds.

(K1) The kernel κ is a density function of bounded variation; $\int |u| \kappa(u) du$ and $\int \kappa(u)^2 du$ are finite. Further, there exists $\delta_{\kappa} > 0$ such that $\min(\int_0^{\delta_{\kappa}} \kappa, \int_{-\delta_{\kappa}}^0 \kappa) > 0$.

Proposition 5.2 (Proposition 1 of Petersen and Müller (2016)). Under assumptions (A1) and (K1), the weighted kernel density estimate \check{p} as defined in (2.10) satisfies (D1) for all $h \rightarrow 0$ and $Nh \rightarrow \infty$ as $N \rightarrow \infty$ with $b_N^2 = h^2 + (Nh)^{-1}$. Condition (D2) is satisfied for any $h = h_N = N^{-r_h}$, $a_N = N^{-r_a}$ as long as $0 < r_h + r_a < 1/2$ with $0 < r_a < r_h$. Moreover, (S1) is satisfied when taking $m(n) = n^{r_m}$ for any $r_m > 0$.

Condition **(K1)** is relatively weak and is satisfied by, e.g., the Gaussian kernel. Moreover, with a proper choice of bandwidth h , e.g., $h \asymp m^{-1/3}$, let $m = m(n) = n^{r_m}$ and take $a_m = n^{-r_a r_m}$, $b_m = n^{-r_m/3}$, then **(D1)**, **(D2)**, and **(S1)** are satisfied. While our theoretical results consider using KDE as per smoother, similar L^∞ and L^2 convergences results for logpline density estimates have been investigated in [Stone \(1990\)](#).

5.2.2 Main Consistent Results

We have the following result for the proposed MLE within $\hat{\mathcal{P}}_K$. Recall that n is the number of training subpopulations, m is the minimal training sample size in **(S1)**, N is the size of the fitting sample, and sequences $\{a_m\}$, $\{b_m\}$ are those in **(D1)** and **(D2)**.

Theorem 5.1. *Under **(A1)**, **(C1)**, **(C2)**, **(D1)**, **(D2)**, and **(S1)**, if n , N , K increase to infinity in such a way that*

$$A_K \sqrt{K/N} \rightarrow 0, \quad KA_K(1/\sqrt{n} + b_m) \rightarrow 0, \quad \sum_{k \leq K} \lambda_k^{-1}(1/\sqrt{n} + a_m) = O(1),$$

$$A_K \sum_{k \leq K} \delta_k^{-1}(1/\sqrt{n} + b_m) \rightarrow 0, \quad \sum_{k \leq K} (\delta_k \lambda_k)^{-1}(1/\sqrt{n} + b_m) = O(1),$$

where

$$A_K = 2 \max \left(|\mathcal{T}|^{-1/2}, \left(\sum_{k=1}^K \|\varphi'_k\|_\infty \right)^{1/3} \right), \quad (5.1)$$

then

$$D(p \parallel \hat{p}_{N,K}) = O_p \left(\left(\frac{1}{n} + b_m^2 \right) \left(K + \sum_{k \leq K} \delta_k^{-1} \right)^2 + \sum_{k > K} \lambda_k + \frac{K}{N} \right).$$

Proof. See [Theorem S4.2](#) in supplementary materials. \square

Note that the result is highly flexible and suits any general infinite dimensional families. In particular, we do not assume the underlying \mathcal{P} to be a finite-dimensional exponential family. The three summands in the rate correspond to the training error, a bias term due to the approximating family, and a variance term from fitting with N observations. Varying the number of components K trades off errors from these three terms, as a more complex model with a larger K will have larger errors from training and fitting, but smaller approximation bias. Quantity A_K is closely related to **(C1)** and the equivalence of L^∞ and L^2 norm in the eigenspaces of covariance operator; for detail, see [Proposition S2.1](#) in supplementary materials.

Our general result directly implies the next corollary where the underlying family is actually a K_0 -dimensional exponential family for some finite K_0 with no approximation bias resulting from truncating the log-densities. Note that **(C1)** is not required, and by convention we set λ_k , φ_k to be zero for $k > K_0$.

Corollary 5.1. Under **(A1)**, **(C2)**, **(D1)**, **(D2)**, and **(S1)**, if \mathcal{P} is a K_0 -dimensional exponential family for some finite K_0 , then for any fixed $K \geq K_0$,

$$D(p \parallel \hat{p}_{N,K}) = O_p \left(\frac{1}{n} + b_m^2 + \frac{1}{N} \right),$$

as $n, N \rightarrow \infty$ and $m = m(n) \rightarrow \infty$.

Proof. See [Corollary S4.1](#) in the supplementary materials. \square

5.2.3 Selecting K

We provide an example when the requirements in [Theorem 5.1](#) are satisfied in the following proposition.

Proposition 5.3. Under **(C2)**, if

- (1) the eigenfunctions coincide with the polynomial or trigonometric basis so that $\|\varphi'_k\|_\infty \asymp k$ while k large;
- (2) eigenvalues have polynomial decay: $\lambda_k \asymp k^{-r}$ with $r \geq 3$ as $k \rightarrow \infty$;
- (3) minimum sizes of the n training sample satisfies $m(n) = n^{r_m}$ for some $r_m > 0$;
- (4) weighted KDE [\(2.10\)](#) is used as pre-smoother with $h \asymp m^{-1/3} = n^{-r_m/3}$ as $n \rightarrow \infty$; and
- (5) for any fixed $0 < r_a < 1/6$, the number of components K used for fitting in dependence on r, n, N, r_m and r_a satisfies

$$K = \hat{K}^* \asymp \min \left(n^{\frac{1}{4(r+1)}}, n^{\frac{r_a r_m}{r+1}}, N^{1/r} \right) \text{ as } n, N \rightarrow \infty,$$

then the conditions for [Theorem 5.1](#) are satisfied with $a_m = n^{-r_a r_m}$, $b_m = n^{-r_m/3}$. As $n, N \rightarrow \infty$,

$$D(p \parallel \hat{p}_{N,\hat{K}^*}) = O_p \left(n^{\gamma_1} + N^{-1+1/r} \right),$$

where $\gamma_1 = r_a r_m (1-r)/(r+1)$ if $r_m \leq 1/(4r_a)$, and $\gamma_1 = -1/4 + 1/(2r+2)$ if $r_m > 1/(4r_a)$.

Proof. See [Proposition S4.2](#) in supplementary materials. \square

Such \hat{K}^* is derived by finding the optimal and feasible K for the dominating terms in the convergence rate. In [Proposition S4.2](#) of supplementary materials, it is suggested that in this example, pre-smoothing step does not slow down the convergence rate for the proposed MLE if the training subpopulations are densely observed so that r_m is large, e.g. $r_m > 3/2$. Since if $r_m > 1/(4r_a)$, then $D(p \parallel \tilde{p}_{N,\hat{K}^*}) \asymp D(p \parallel \hat{p}_{N,\hat{K}^*})$ with an optimal \hat{K}^* for MLE within $\tilde{\mathcal{P}}_K$.

This result is particularly interesting since it suggests that, for better convergence rate, when pre-smoothing with KDE, slight over-smoothing may be preferred. Indeed, noting $\gamma_1 < 0$ will be smaller if $r_a r_m > 1/4$, it is desirable to have larger r_a so that smaller r_m can satisfy $r_a r_m > 1/4$, which means smaller training samples can be considered “dense”. As required in [Proposition 5.2](#), the only restrictions for r_a are $0 < r_h + r_a < 1/2$ and $0 < r_a < r_h$, and hence if we choose a smaller $r_h > 1/4$, a larger r_a would be possible, making $r_a r_m > 1/4$ easier to satisfy.

5.3 Consistency of Component Scores

Another interesting question is the convergence of the component scores of pre-smoothed training trajectories $\check{f}_i = \psi \check{p}_i$, $i = 1, \dots, n$, which are used to capture distribution of random densities in MAP [\(2.13\)](#) and BLUP [\(2.14\)](#). Notation-wise, let $\check{f}_{i,K} = \hat{\mu} + \sum_{k \leq K} \check{\eta}_{ik} \hat{\varphi}_k$ be the truncated pre-smoothed log-density with $\check{\eta}_{ik} = \langle \check{f}_i - \hat{\mu}, \hat{\varphi}_k \rangle$ for $k = 1, \dots, K$, $i = 1, \dots, n$. The next proposition shows that the estimated component scores $\check{\eta}_{ik}$ converge uniformly to the truth $\eta_{ik} = \langle f_i - \mu, \varphi_k \rangle$.

Proposition 5.4. Under [\(A1\)](#), [\(D1\)](#), [\(D2\)](#), [\(S1\)](#), and [\(C2\)](#), for any $K < \infty$, as $n \rightarrow \infty$, we have

$$\sup_{i \leq n} \sup_{k \leq K} |\check{\eta}_{ik} - \eta_{ik}| = O_p(a_m + (n^{-1/2} + b_m) \sup_{k \leq K} \delta_k^{-1}).$$

Proof. See [Proposition S3.4](#) of supplementary materials. □

With the previous proposition, it is easy to see $\sup_{i \leq n} \sup_{k \leq K} |\check{\eta}_{ik} - \eta_{ik}| = O_p(a_m + n^{-1/2})$ as $n \rightarrow \infty$ if K is fixed. To have a similar result with $K \rightarrow \infty$ as well, we need $n, K \rightarrow \infty$ in such a way that $(n^{-1/2} + b_m) \sup_{k \leq K} \delta_k^{-1} \rightarrow 0$. Under the conditions of [Proposition 5.3](#), we can set $K \asymp n^\beta$ for any $\beta < \max(1/2, r_m/3)/(1+r)$, then the sample component scores are consistent uniformly. In particular, $K = \hat{K}^*$ satisfies the requirement.

A Scaling the Responses for Heavy-tailed Densities

Suppose that the original responses $\{Y_{ij} \in \mathbb{R}^+ : i = 1, \dots, n; j = 1, \dots, N_i\}$ have a heavy right-tail and the pre-smoothing density estimates for the training sub-populations are occasionally zero, which will create an issue when considering log-densities. To address this issue, we log-scale the responses and obtain $X_{ij} \stackrel{\Delta}{=} \log Y_{ij}$ lying in a compact working domain $\mathcal{T} \stackrel{\Delta}{=} [0, \max(X_{ij}) + \delta]$ for some adjustment $\delta > 0$. Using generic notations, denote Y as the random variable associated with responses in original scale with density $p_Y(y)$ for $y > 0$, and the density of $X \stackrel{\Delta}{=} \log Y$ as $p_X(x)$ for $x \in \mathcal{T}$.

The proposed methods now proceed by applying the FPCA to the transformed trajectories $f_{X,i} = \psi p_{X,i}$, $i = 1, \dots, n$, leading to mean function μ_X and eigenfunctions $\varphi_{X,k}$, $k \in \mathbb{N}^+$, with which we construct approximating families for the distribution of X , whose density functions would take form of

$$p_{X,\theta}(x) \propto \exp \left(\mu_X(x) + \sum_{k=1}^K \theta_k \varphi_{X,k}(x) \right), x \in \mathcal{T},$$

where $\theta_1, \dots, \theta_K$ are natural parameters. In the end, reverse the log-scaling to arrive at approximating families for distribution of Y , densities in which take form of

$$p_{Y,\theta}(y) \propto \exp \left(\mu(\log y) - \log y + \sum_{k=1}^K \theta_k \varphi_k(\log y) \right), y \in \mathbb{R}^+.$$

The distribution of component scores is preserved before and after scaling, since all parameters $\theta_1, \dots, \theta_K$ are unchanged from $p_{X,\theta}$ to $p_{Y,\theta}$, making the proposed MAP and BLUP methods still valid.

Supplement to “Nonparametric Estimation of Repeated Densities with Heterogeneous Sample Sizes”. The supplementary materials including details of the theoretical results will be available after publication.

References

Sourabh Aggarwal, Arman Qamar, Vishal Sharma, and Alka Sharma. Abdominal aortic aneurysm: A comprehensive review. *Experimental & Clinical Cardiology*, 16(1):11–15, 2011. ISSN 1205-6626.

Shun-ichi Amari. *Information Geometry and Its Applications*, volume 194 of *Applied mathematical sciences*. Springer, [Tokyo], 2016. ISBN 978-4-431-55977-1 978-4-431-55978-8. doi: 10.1007/978-4-431-55978-8.

Shun-ichi Amari and Hiroshi Nagaoka. *Methods of Information Geometry*, volume 191 of *Translations of mathematical monographs*. American Mathematical Society, Providence, RI; Oxford University Press, Oxford, 2000. ISBN 0-8218-0531-2. doi: 10.1090/mmono/191.

Billie Bonevski, Madeleine Randell, Chris Paul, Kathy Chapman, Laura Twyman, Jamie Bryant, Irena Brozek, and Clare Hughes. Reaching the hard-to-reach: a systematic review of strategies for improving health and medical research with socially disadvantaged groups. *BMC medical research methodology*, 14(1):42, 2014.

Cody Carroll, Alvaro Gajardo, Yaqing Chen, Xiongtao Dai, Jianing Fan, Pantelis Z. Hadjipantelis, Kyunghee Han, Hao Ji, Hans-Georg Mueller, and Jane-Ling Wang. fdapace: Functional data analysis and empirical dynamics. 2020.

Ba Chu, Kim Huynh, David Jacho-Chávez, and Oleksiy Kryvtsov. On the evolution of the United Kingdom price distributions. *Ann. Appl. Stat.*, 12(4):2618–2646, 2018. ISSN 1932-6157. doi: 10.1214/18-AOAS1172.

P. Delicado. Dimensionality reduction when data are density functions. *Comput. Statist. Data Anal.*, 55(1):401–420, 2011. ISSN 0167-9473. doi: 10.1016/j.csda.2010.05.008.

J. J. Egozcue, J. L. Díaz-Barrero, and V. Pawlowsky-Glahn. Hilbert space of probability density functions based on Aitchison geometry. *Acta Math. Sin. (Engl. Ser.)*, 22(4):1175–1182, 2006. ISSN 1439-8516. doi: 10.1007/s10114-005-0678-2.

R. A. Fisher and L. H. C. Tippett. Limiting forms of the frequency distribution of the largest or smallest member of a sample. *Mathematical Proceedings of the Cambridge Philosophical Society*, 24(2):180–190, April 1928. ISSN 1469-8064, 0305-0041. doi: 10.1017/S0305004100015681.

William Fithian and Stefan Wager. Semiparametric exponential families for heavy-tailed data. *Biometrika*, 102(2):486–493, 2015. ISSN 0006-3444. doi: 10.1093/biomet/asu065.

Daniel Gervini. Independent component models for replicated point processes. *Spat. Stat.*, 18(part B):474–488, 2016. doi: 10.1016/j.spasta.2016.09.006.

Daniel Gervini and Manoj Khanal. Exploring patterns of demand in bike sharing systems via replicated point process models. *J. R. Stat. Soc. Ser. C. Appl. Stat.*, 68(3):585–602, 2019. ISSN 0035-9254.

Eric Gilleland and Richard W. Katz. extRemes 2.0: An extreme value analysis package in R. *Journal of Statistical Software*, 72(8):1–39, 2016. doi: 10.18637/jss.v072.i08.

B. Gnedenko. Sur la distribution limite du terme maximum d'une série aléatoire. *Ann. of Math. (2)*, 44:423–453, 1943. ISSN 0003-486X. doi: 10.2307/1968974.

Kyunghee Han, Hans-Georg Müller, and Byeong U. Park. Additive functional regression for densities as responses. *J. Amer. Statist. Assoc.*, 115(530):997–1010, 2020. ISSN 0162-1459. doi: 10.1080/01621459.2019.1604365.

K. Hron, A. Menaoglio, M. Templ, K. Hrůzová, and P. Filzmoser. Simplicial principal component analysis for density functions in Bayes spaces. *Computational Statistics & Data Analysis*, 94:330–350, February 2016. ISSN 0167-9473. doi: 10.1016/j.csda.2015.07.007.

Kim P. Huynh, David T. Jacho-Chávez, Robert J. Petrunia, and Marcel Voia. Functional principal component analysis of density families with categorical and continuous data on Canadian entrant manufacturing firms. *J. Amer. Statist. Assoc.*, 106(495):858–878, 2011. ISSN 0162-1459. doi: 10.1198/jasa.2011.ap10111.

Alistair E. W. Johnson, Tom J. Pollard, Lu Shen, Li-wei H. Lehman, Mengling Feng, Mohammad Ghassemi, Benjamin Moody, Peter Szolovits, Leo Anthony Celi, and Roger G. Mark. MIMIC-III, a freely accessible critical care database. *Scientific Data*, 3(1):1–9, May 2016. ISSN 2052-4463. doi: 10.1038/sdata.2016.35.

Steven G. Johnson. The NLOpt nonlinear-optimization package, 2020.

Dongwoo Kim, Young Kyung Lee, and Byeong U. Park. Principal component analysis for Hilbertian functional data. *Communications for Statistical Applications and Methods*, 27(1):149–161, January 2020. ISSN 2383-4757. doi: 10.29220/CSAM.2020.27.1.149.

Alois Kneip and Klaus J. Utikal. Inference for density families using functional principal component analysis. *J. Amer. Statist. Assoc.*, 96(454):519–542, 2001. ISSN 0162-1459. doi: 10.1198/016214501753168235.

Charles Kooperberg and Charles J. Stone. A study of logspline density estimation. *Comput. Statist. Data Anal.*, 12(3):327–347, 1991. ISSN 0167-9473. doi: 10.1016/0167-9473(91)90115-I.

Gyemin Lee and Clayton Scott. EM algorithms for multivariate Gaussian mixture models with truncated and censored data. *Comput. Statist. Data Anal.*, 56(9):2816–2829, 2012. ISSN 0167-9473. doi: 10.1016/j.csda.2012.03.003.

Clive R. Loader. Local likelihood density estimation. *Ann. Statist.*, 24(4):1602–1618, 1996. ISSN 0090-5364. doi: 10.1214/aos/1032298287.

Victor M. Panaretos and Yoav Zemel. Amplitude and phase variation of point processes. *Ann. Statist.*, 44(2):771–812, 2016. ISSN 0090-5364. doi: 10.1214/15-AOS1387.

Alexander Petersen and Hans-Georg Müller. Functional data analysis for density functions by transformation to a Hilbert space. *Ann. Statist.*, 44(1):183–218, 2016. ISSN 0090-5364. doi: 10.1214/15-AOS1363.

R.-D. Reiss and M. Thomas. *Statistical Analysis of Extreme Values with Applications to Insurance, Finance, Hydrology and Other Fields*. Birkhäuser Verlag, Basel, third edition, 2007. ISBN 978-3-7643-7230-9.

S. J. Sheather and M. C. Jones. A reliable data-based bandwidth selection method for kernel density estimation. *J. Roy. Statist. Soc. Ser. B*, 53(3):683–690, 1991. ISSN 0035-9246.

A. Srivastava, I. Jermyn, and S. Joshi. Riemannian analysis of probability density functions with applications in vision. In *2007 IEEE Conference on Computer Vision and Pattern Recognition*, pages 1–8, 2007.

Charles J. Stone. Large-sample inference for log-spline models. *Ann. Statist.*, 18(2):717–741, 1990. ISSN 0090-5364. doi: 10.1214/aos/1176347622.

Ruey S. Tsay. Some methods for analyzing big dependent data. *J. Bus. Econom. Statist.*, 34(4):673–688, 2016. ISSN 0735-0015. doi: 10.1080/07350015.2016.1148040.

Jon Wakefield and Paul Elliott. Issues in the statistical analysis of small area health data. *Statistics in Medicine*, 18(17-18):2377–2399, 1999.

Shuang Wu, Hans-Georg Müller, and Zhen Zhang. Functional data analysis for point processes with rare events. *Statist. Sinica*, 23(1):1–23, 2013. ISSN 1017-0405.

Fang Yao, Hans-Georg Müller, and Jane-Ling Wang. Functional data analysis for sparse longitudinal data. *J. Amer. Statist. Assoc.*, 100(470):577–590, 2005. ISSN 0162-1459. doi: 10.1198/016214504000001745.

Shui-qing Yin, Zhonglei Wang, Zhengyuan Zhu, Xu-kai Zou, and Wen-ting Wang. Using Kriging with a heterogeneous measurement error to improve the accuracy of extreme precipitation return level estimation. *Journal of Hydrology*, 562:518–529, July 2018. ISSN 0022-1694. doi: 10.1016/j.jhydrol.2018.04.064.

Da-Lin Zhang, Yonghui Lin, Ping Zhao, Xiaoding Yu, Songqiu Wang, Hongwen Kang, and Yihui Ding. The Beijing extreme rainfall of 21 July 2012: “right results” but for wrong reasons. *Geophysical Research Letters*, 40(7):1426–1431, 2013. ISSN 1944-8007. doi: 10.1002/grl.50304.